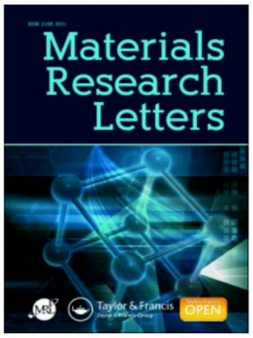

Materials Research Letters

ISSN: 2166-3831 (Online) Journal homepage: www.tandfonline.com/journals/tmrl20

Non-destructuve 3D microstructure mapping for large samples with complex microstructure

M. Carlsen, W. Hearn, A. Acharya, U. Lienert, S. Van Petegem & M. Liebi

To cite this article: M. Carlsen, W. Hearn, A. Acharya, U. Lienert, S. Van Petegem & M. Liebi (2026) Non-destructuve 3D microstructure mapping for large samples with complex microstructure, Materials Research Letters, 14:1, 107-114, DOI: 10.1080/21663831.2025.2591884

To link to this article: https://doi.org/10.1080/21663831.2025.2591884

Published online: 27 Nov 2025.

MATER. RES. LETT.
2026, VOL. 14, NO. 1, 107–114
https://doi.org/10.1080/21663831.2025.2591884

MATERIALS RESEARCH LETTERS
Taylor & Francis
Taylor & Francis Group

Non-destructuve 3D microstructure mapping for large samples with complex microstructure

M. Carlsen[a], W. Hearn[a], A. Acharya[a,b], U. Lienert[c], S. Van Petegem[a] and M. Liebi[a,b]

[a]Center for Photon Science, Paul Scherrer Institute (PSI), Villigen, Switzerland; [b]Institute of Materials, Ècole Polytechnique Fèdèrale de Lausanne, Lausanne, Switzerland; [c]DESY Photon Science, Hamburg, Germany

ABSTRACT
Scanning 3D x-ray diffraction is a non-destructive synchrotron technique for mapping the 3D microstructure of polycrystalline materials where a focused hard x-ray beam is scanned across the sample to obtain spatially-resolved microstructure information. We demonstrate a new approach to such an experiment which extends the capabilities of existing techniques to be able to handle more complex and highly deformed microstructures. We demonstrate this by mapping the formation of sub micro meter sized deformation twins in-situ and in the bulk at deformation levels up to 20% in an as-built additively manufactured steel sample.

ARTICLE HISTORY
Received 15 September 2025

KEYWORDS
Three-dimensional X-ray diffraction; additive manufacturing; plasticity

1. Introduction

Predictive modeling of deformation mechanics of polycrystaline materials on the meso scale involving grain-grain interactions, deformation twinning, and the development of sub-grains remains a challenge. Validation of these models mainly relies on macroscopic properties and comparison with either surface measurements or destructive 3D maps made by serial sectioning. *In-situ* datasets where the evolution of the microstructure can be followed at the grain-level are needed to test the accuracy of existing models and guide ongoing development.

Synchrotron x-ray techniques for microstructure imaging such as three dimensional x-ray diffraction makes such measurements possible and has proven to be a useful tool for investigating a range of phenomena in polycrystalline metals. The range of 3D x-ray grain-mapping techniques can be split into four groups.

(1) Far-field techniques, that utilize a large field of illumination and achieve high orientation and strain resolution. However, they do not recover the shape of the grains nor the inter-granular variation [1,2].
(2) Near-field techniques that use the shape of Bragg-peaks and extinction contrast of the transmitted beam to reconstruct the shape of the grains, and to some degree inter-granular misorientations [3–5].
(3) Methods that use optical components inserted downstream of the sample to achieve better both spatial and orientational resolution, such as differential aperture microscopy [6] and dark-field x-ray microscopy [7].
(4) A new approach based on scanning a micro-focused x-ray beam over the sample(s3D-XRD) [8,9] has become popular thanks to improvements of x-ray sources and detectors that allow ever faster scanning.

s3D-XRD has in recent years been used to study a range of phenomena such as grain growth [9], dissolution and sintering [10], and plastic deformation [11]. A major limitation of the existing algorithms is the need to be able to do peak-segmentation on the recorded the diffraction patterns, which limits the application to small inter granular misorientation and large grains, relative to the x-ray beam size. Recent improvements to the reconstruction algorithms have made it possible to map volumes with larger inter granular misorientations [12] and a higher number of grains [13]. Similarly, efforts have been made in the techniques utilizing a wide field of illuminations by utilizing the shape of diffraction peaks in the far field to determine per-grain orientation distributions [14] and by combining this with near-field measurements to achieve intragranular orientation resolution [15]. Nevertheless, the methods still remain largely limited to studying fully recrystallized microstructures or samples containing a small number of moderately deformed grains.

To overcome this issue, it has recently been suggested to use texture tomography(TT) [16,17] as an alternative

CONTACT M. Carlsen mads.carlsen@psi.ch PSI Center for Photon Science Paul Scherrer Institute PSI, Forschungsstrasse 111, 5232 Villigen PSI, Switzerland

approach to reconstruct s3D-XRD data. The main advantage of TT that it is able to handle samples with grains smaller than the size of the focused x-ray beam. This is possible as TT allows multiple orientations to be present in a single reconstruction voxels. This however comes at the cost of reduced orientation resolution.

To demonstrate the viability of this approach, we use a sample that is challenging for the existing grain-mapping techniques. Additively manufactured metals commonly contain a mix of very large columnar grains with large inter granular misorientation, and regions with small equiaxed grains [18,19]. The twinning induced plasticity(TWIP) effect results in the creation of sub-micron sized crystalline domains adding another complication to the reconstruction of the microstructure. The characterization of such a sample with the established algorithms would therefore require a sub-micron x-ray beam and a large number of scan-points. With TT these restrictions are loosened allowing large samples to be mapped with a coarser resolution.

Deformation studies, such as the one presented in this paper were one of the early successes of the original far-field techniques [20–22] where the reorientation of individual grains could be tracked over large plastic deformation. Studies with inter granular resolution have also been demonstrated with s3D-XRD [11,12] with fully recrystallized initial microstructures. Studies involving more complicated micro structures, such as is present in additively manufactured metals, are rare [23–26] and have relied on heat-treating the sample to study annealed or recovered grains, rather than the as-built microstructure.

We perform an interrupted tensile-loading of a tensile specimen up to 20% reduction of the cross-section and track the evolution of individual grains and the development of twin lamella. The sample is an additively manufactured 304L stainless steel sample that was produced by laser powder bed fusion(LPBF).

2. Method

2.1. Sample synthesis

The sample is a dog bone shaped tensile specimen of 304L stainless steel that was produced by LPBF using a custom-built machine [27]. For the 304L stainless steel alloy, gas-atomized powder (supplied by Carpenter Additive, United Kingdom) was used that had a mean particle size of 45 microns and a composition of Fe-18.4Cr-9.8Ni-1.4Mn-0.61Si–0.1Cu-0.07N-0.03O-0.015C-0.012P-0.004S. Using this powder, a 12 × 12 × 12 mm cube was printed with a laser spot size of 45 μm and a power of 250 W using a TruFiber 500 P compact (FD44-W) fiber laser (TRUMPF Schweiz AG, Switzerland). The cube was printed with a scan speed of 600 mm/s, a hatch spacing of 45 μm, and a layer thickness of 30 μm, where the scan-lines were rotated by 90° between each layer. During processing, the chamber of the LPBF machine was filled with high purity argon gas (99.998%) to maintain an oxygen level below 0.2% After printing, the produced cube was electrical discharge machined (EDM) to make the tested tensile specimens that had a nominal cross section 1 × 2 mm. Following EDM, the samples were polished using P4000 SiC grit paper to remove surface damage caused by EDM.

2.2. X-ray experiment

The experiments were performed at the beamline P21.2 at the synchrotron source PETRA III at DESY in Hamburg, Germany. The experiment utilizes a focused x-ray beam of approximately 5 μm vertical and 6 μm horizontal full width at half maximum at a photon energy of 82 keV. The sample was scanned in steps of 6 μm horizontally and under continuous rotations with 360 measured diffraction patterns spaced out over a 180° rotation.

The diffraction patterns were measured using a flat panel detector(4343CT, Varex Imaging, USA) and the sample was deformed using an open frame deformation rig(CT20K, Deben, UK). The deformation was performed in steps up to a certain plastic elongation of the sample and the measurements were performed while the sample was unloaded.

The tomographic measurement of each slice consists of 401 such 180° rotations for a total of about 72,000 diffraction patterns which took 5 hours to measure. The measurement speed was limited by the time-resolution of the x-ray detector at 15 frames per second as well as significant overheads from motor movements.

2.3. Texture-tomography reconstructions

From the measured diffraction patterns, the radially integrated intensities of the eight observed Bragg peaks were computed for 720 azimuthal bins using the open-source software-package pyFAI [28] giving a total of 5760 diffraction sinograms.

The sample is modeled by a pixel-map where a full orientation distribution function(ODF) is represented in each pixel [17]. The forward model involves computing the diffraction intensity from each ODF and summing over the intensity from each voxel along a line, using standard algorithms from texture analysis and computed tomography respectively. The model is then fitted to the data using gradient descent. The texture is represented with radial basis functions using a grid with about ten

thousand orientations in the asymmetric zone of the cubic lattice. The gradient descent algorithm was run for 200 iterations. The converged solutions are highly sparse, with respectively 0.6% and 1.0% non-zero coefficients for the initial and final strain steps respectively.

2.4. Analysis of texture-tomography reconstructions

The pixel wise ODFs were first subjected to a clustering algorithm to find a number of distinct texture-components in each voxel. For each such component a mean orientation and a density is computed. In most pixels, a single texture component was found with density above the chosen threshold, but at grain boundaries and regions with small-grains, multiple texture component were found.

For each pixel with multiple texture components, an intra-pixel misorientation was computed between the orientations with the highest and second-highest densities. In the final deformed reconstruction, voxels displaying a misorientation less than 7° from the spinel twinning law (60° rotation about a ⟨111⟩-axis) were considered to display TWIP. The cutoff of 7° was chosen to capture the full width of the peak in a histogram of the misorientation magnitude and is somewhat larger than the grid-resolution of the texture model (nearest neighbor distance of 5°). Texture components in neighboring pixels with less than 3° misorientation were then grouped into grains.

2.5. Grain tracking

To follow the evolution of individual grains, it is necessary to identify the same grain across the different reconstructions. To do this, first a number of recognizable features, such as sample edges, pores in the interior (caused by lack of fusion defects), and certain large grains were identified in all three reconstructions manually. From this set of points, a two dimensional deformation-field, modeled by a second order polynomial, was fitted. Following this, a search was performed for each grain in the initial structure at the corresponding positions after deformation in the deformed reconstructions. Any grain with its center-of-mass in this region and with a misorientation relative to the initial grain of less than 15° and a similar size is considered a match. 52 such grains were matched between all three tomograms.

2.6. EBSD measurements

The *in-situ* sample was investigated after deformation by electron back-scattering diffraction (EBSD). Prior to EBSD measurements, specimens were initially sectioned using a wire-saw and subsequently hot mounted in conductive resin using a SimpliMet 1000 machine (Buehler, USA). These specimens were subsequently ground using SiC paper from a grit of P320 down to P4000 before being polished down to a 1 μm diamond suspension using a LaboForce-100 machine (Struers, Denmark) before final polishing using OPS solution. EBSD measurements were carried out using an Ultra 55 SEM (Zeiss, Germany) scanning electron microscope (SEM) that was equipped with an EDAX EBSD detector (Hikari, Japan). EBSD analysis was done on the OPS polished specimens using an accelerating voltage of 20 kV and at step sizes of 100 and 800 nm to examine deformed and undeformed regions. The collected EBSD data was analyzed using TSL OIM Analysis 8.1.0 software.

3. Results

We have obtained three texture tomography measurements of a cross section near the middle of the tensile specimen with 6 μm resolution, corresponding to the initial structure, and deformed samples at 10%, and 20% reduction of the sample cross section. The cross section of the undeformed sample was measured to be 1.9 × 0.9 mm and was oriented with the build direction(BD) of the sample along the longer dimension of the cross section. (See Figure 1(a))

For each scan, an averaged powder diffraction pattern was generated by integrating the 2D diffraction data over all orientations and scan points. The resulting profiles were analyzed using the modified Williamson–Hall (mWH) method [29], where dislocation contrast factors are employed to account for the anisotropic broadening of the diffraction peaks. Figure 1(b) shows the corresponding mWH plots for the undeformed sample and after the first and second deformation steps. In all cases, the data align well along straight lines, indicating that the anisotropic broadening can be consistently attributed to the presence of dislocations. The increasing slope clearly reflects a rise in dislocation density with strain. Additional anisotropic broadening effects expected from deformation twins, as described by Warren's theory [30], were not observed—presumably due to an insufficient twin density to measurably impact the diffraction profiles.

We obtain a tomographic reconstruction of the local texture consisting of an ODF in each pixel of the tomogram. Throughout most of the sample, the grains are well-resolved allowing us to compute an orientation field which is plotted as an load direction (LD) inverse pole figure(IPF) map in Figure 1(c-e). As a result of the deformation, the sample becomes macroscopically warped and

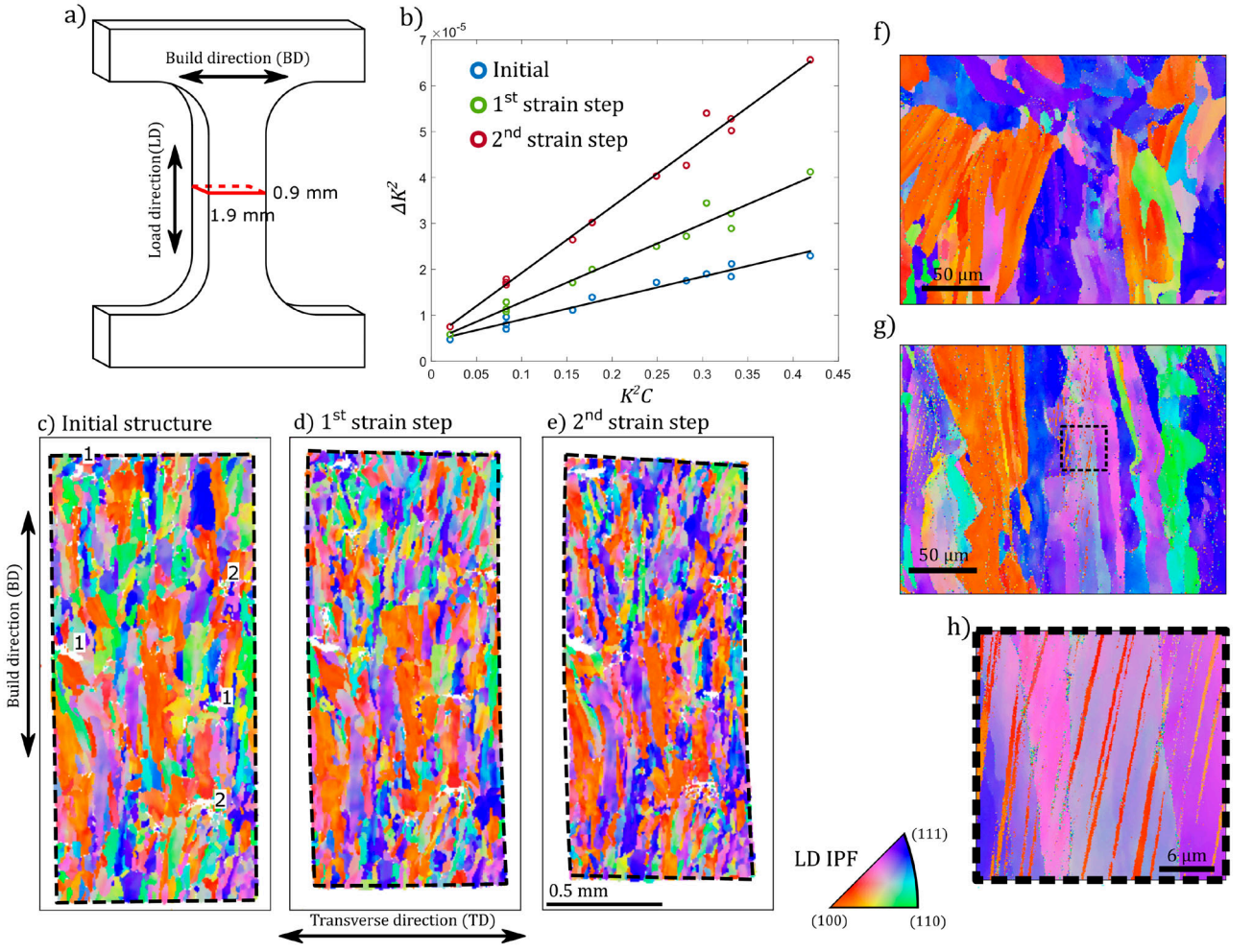

Figure 1. Texture tomography reconstructions of 2D cross sections. (a) Sketch of the sample geometry with the approximate location of the measured cross-section. (b) Modified Williamson-Hall plots for the three measurements showing increasing peak-broadening due to dislocations. K refers to the magnitude of the diffraction vector, ΔK is the peak-width and C is the dislocation contrast-factor. (c–e) reconstructed main orientation for (c) the initial structure, (d) after the first, and (e) after the second strain-step plotted as LD IPF maps. In (c) areas with lack-of-fusion defects and small equiaxed grains are marked with (1) and (2) respectively. (f–h) show EBSD maps of the sample in (f) an undeformed region and (g) a deformed region (h) shows a zoomed in view of a region displaying twinning.

grains are visibly reoriented. The measurement is only of a single 2D cross section with a height defined by the height of the x-ray beam of 5 µm. Because the sample warps, the slices measured in the three scans are not identical, but several sample features such as lack-of-fusion defects, regions with fine equiaxed grains, and individual large grains can be recognized across the three tomograms, suggesting that the offset between the slices is less than the LD size of the larger grains of around 50 µm.

Despite this complication, a number of larger grains can be tracked across all three tomograms. Figure 2(a,b) shows two such grains. From these tracked grains, certain average trends are observable. Mainly, a large reorientation of grains initially aligned with ⟨110⟩||LD towards ⟨111⟩||LD, which is common for FCC metals [20–22], including austenic TWIP steel [31,32]. Although internal defects such as lack-of-fusion pores are known to create local stress concentrations and strain heterogeneity [33], these defects were relatively sparse within the analyzed volume. Conversely, the orientation changes observed during loading were widespread and not confined to regions adjacent to defects, suggesting that the deformation behavior is not dominated by these features. Furthermore, as-built LBPF samples are known to contain large residual stresses due the high cooling rates during solidification [34]. Such residual stresses could influence the lattice reorientation during early stages of deformation. While we do not recover the lattice strain in the present reconstruction workflow, such a strain reconstruction has been shown to be possible with peak-segmentation based methods [35].

We also observe TWIP occurring between the second and the third scan. While the narrow twin lamella are not spatially resolved by the experiment, we can observe the

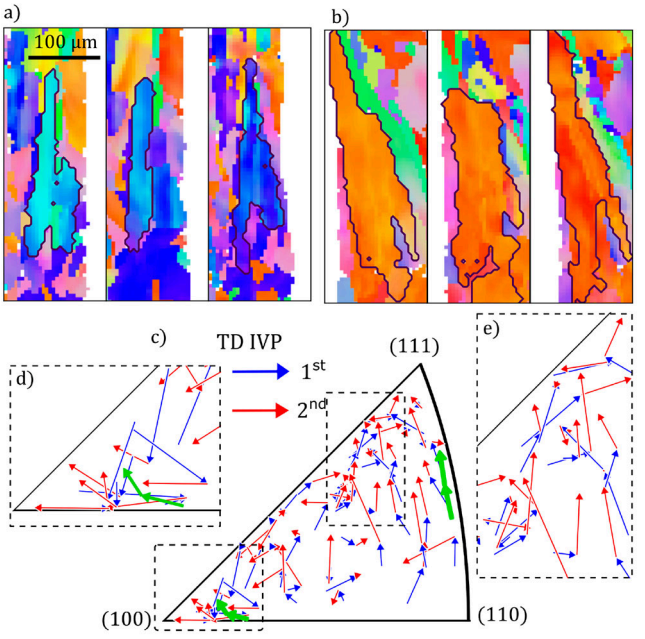

Figure 2. Orientation changes in tracked grains. (a,b) LD IPF-maps of two tracked grains in the initial, 1st strained, and 2nd strained reconstructions from left to right. (c) Mean orientation changes of all tracked grains plotted as arrows on the TD IPF. The two grains in (a,b) are highlighted in green. (d,e) Magnified view of regions in (c).

twinning as intra-pixel misorientations by reconstructing several orientations within a single voxel. Figure 3(a–c) shows histograms of the misorientation magnitude for all pixels with multiple orientations present. In all three cases, the histograms are dominated by pixels close to grain boundaries, where the orientations of neighboring grains blur together. The first two histograms follow a random distribution except for an over representation of low angle grain boundaries. In the histogram from the final scan, there is furthermore a peak at 60° which corresponds to the spinel twin law given by a 60° rotation about a ⟨111⟩ axis.

Figure 3(d) shows the spatial distribution of pixels displaying twinning and the orientation of the major texture component as LD-IPF color. Figure 3(e,f) show these orientations as scatter plots in an LD-IPF. The major texture component is concentrated around ⟨111⟩||LD while the minor component is concentrated near ⟨100⟩||LD. The volume fraction of the minor component displays a distribution around 20%–30% while the pixels with misorientations attributed to grain boundaries have volume fractions around 50% (Figure 3(h,i)). Volume fractions lower than about 20% are not identified by the analysis due to the threshold used to identify texture components from the ODFs. This means that we do not

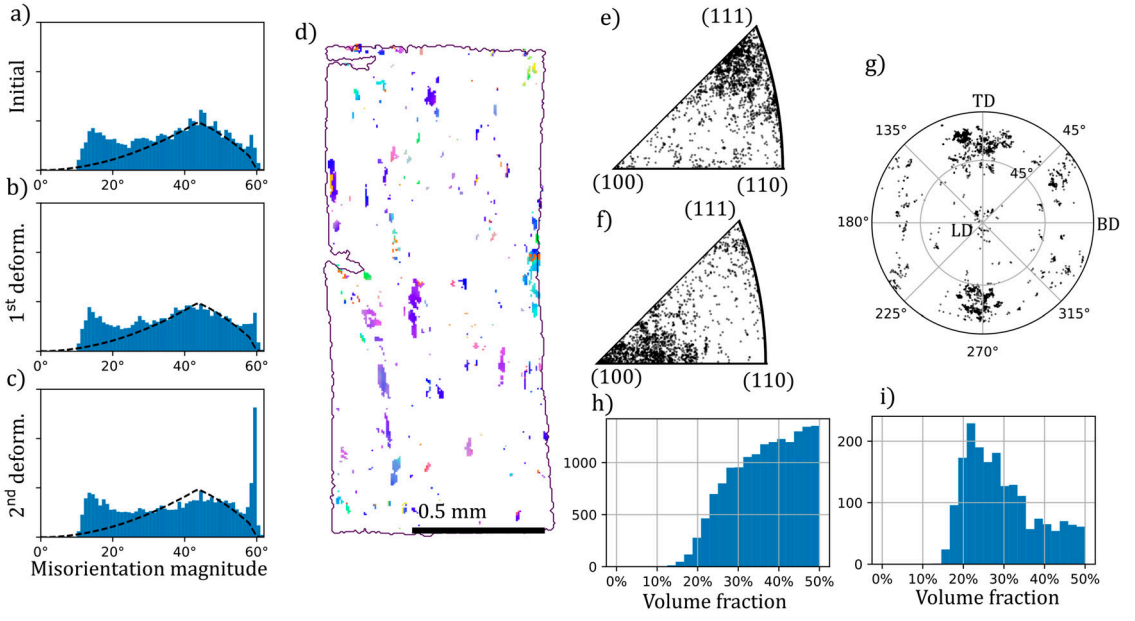

Figure 3. Observation of TWIP. (a–c) histograms of intra-pixel misorientations (a) in the initial state, (b) after the first deformation, and (c) after the second deformation. (d) spatial distribution of the grains displaying TWIP (e) major- and (f) minor texture components shown as a scatter plot on the LD IPF. (g) pole figures of the misorientation axis. Histograms of the volume fraction of the minor component in (h) pixels displaying two orientation but not close to the twin law and (i) close to the twin law.

find volumes with only a small volume fraction of twin lamella and therefore likely underestimate the area that displays twinning. We can also observe the direction of the misorientation axis relative to the sample coordinates. Figure 3(g) shows that twinning primarily occurs along [111] planes that have an angle at around 60° relative to the LD and 90° relative to the build direction. While the orientation relative to the load direction is explained by the mechanical criteria for twin formation, the preferred orientation relative to the build direction can only be explained by the preexisting microstructure. We note that the preferred 90° orientation observed corresponds to twin lamella parallel to the long direction of the grains, while the avoided 0° orientation would give twin domains roughly orthogonal to the long direction. Consistent with the understanding that deformation twinning occurs more readily in larger-grained materials [36]. This is also observed in the EBSD maps shown in Figure 1, where the twins appear as stripes close to parallel with BD (vertical).

Where the twinned grains can be identified with one of the tracked grains from the earlier scans, it appears in all cases that an ⟨111⟩||LD exists beforehand (in the initial structure and after the first deformation step) and the orientation ⟨100⟩||LD appears as a result of twinning in line with the prevailing understanding [31,32]. One such tracked grain, that displays both slip and TWIP is shown in Figure 4.

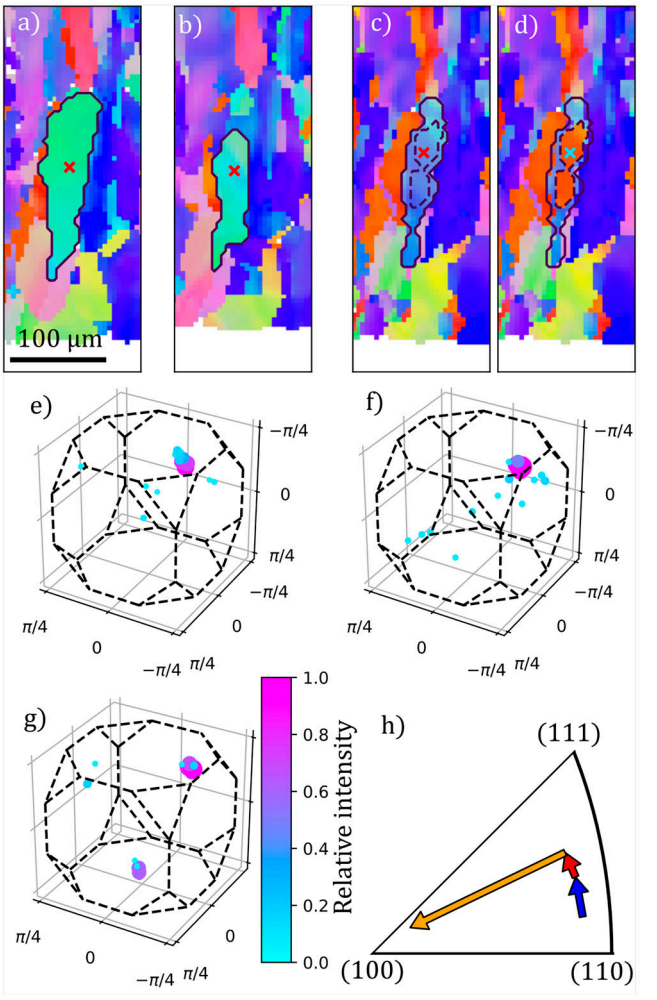

Figure 4. Close up of a single grain displaying both slip and TWIP effects. (a–d) LD IPF maps of the selected grain in the (a) initial state, (b) after the first deformation, and (c,d) after the second deformation highlighting respectively the primary and secondary orientations. (e-g) ODFs in Rodriguez-vector representation for the (e) initial, (f) first, and (g) second deformed measurements. The ODFs correspond to the single voxels marked by a cross in the corresponding maps (a–c). (h) Load direction IPF representation of the texture components in (e–g). The arrows represent the lattice reorientation due to slip (blue and red) and TWIP (orange).

4. Conclusion

The results presented in this paper show promise for texture tomography as an alternative approach to reconstructing s3D-XRD data sets for samples with large inter granular misorientation and unresolved micro structural features. We have demonstrated the feasibility of such an experiment by performing an interrupted tensile loading experiment on a sample of LBPF 304L steel up to 20% reduction of cross section. We observe the expected reorientation of lattice towards LD||{111} and the development of deformation twins preferentially in grains at LD||{111} orientation.

The large deformation of the sample between each measurement and the resulting uncertainty in the position of the measured cross section along LD leads to difficulty in analyzing the results. The experiment would therefore benefit from a full 3D measurement, which can be achieved by translating the sample along LD and repeating the measurement. While the present experiment was limited by the speed of the flat-panel detector used, we estimate that by using a faster detector and eliminating overheads, it should be possible to get measurement times of similarly sized samples down to below 10 minutes per cross section, allowing full 3D measurements within acceptable experimental time.

Acknowledgments

We acknowledge DESY (Hamburg, Germany), a member of the Helmholtz Association HGF, for the provision of experimental facilities. Parts of this research were carried out at PETRA III and we would like to thank Dr. Z. Hegedüs and Sven Gutschmidt for assistance in using P21.2. Beamtime was allocated for proposal I-20240222 EC.

Disclosure statement

No potential conflict of interest was reported by the author(s).

Funding

MC has received funding from the European Union's Horizon 2020 Research and Innovation Program under the Marie Skłodowska-Curie grant agreement No 884104. SVP and WH has received funding from the Swiss National Science Foundation (SNSF) (Grant No. CRSII5_193799). ML has received funding from the European Research Council (ERC-2020-StG 949301 MUMOTT). Views and opinions expressed are however those of the author(s) only and do not necessarily reflect those of the European Union or the European Research Council Executive Agency. Neither the European Union nor the granting authority can be held responsible for them.

References

[1] Lauridsen EM, Schmidt S, Suter RM, et al. Tracking: a method for structural characterization of grains in powders or polycrystals. J Appl Crystallogr. 2001 Dec;34(6):744–750. doi: 10.1107/S0021889801014170

[2] Poulsen HF, Nielsen SF, Lauridsen EM, et al. Three-dimensional maps of grain boundaries and the stress state of individual grains in polycrystals and powders. J Appl Crystallogr. 2001 Dec;34(6):751–756. doi: 10.1107/S0021889801014273

[3] Suter RM, Hennessy D, Xiao C, et al. Forward modeling method for microstructure reconstruction using X-ray diffraction microscopy: single-crystal verification. Rev Sci Instrum. 2006 Dec;77(12):123905. doi: 10.1063/1.2400017

[4] Johnson G, King A, Honnicke M, et al. X-ray diffraction contrast tomography: a novel technique for three-dimensional grain mapping of polycrystals. II. The combined case. J Appl Crystallogr. 2008;41(2):310–318. doi: 10.1107/S0021889808001726

[5] Ludwig W, Schmidt S, Lauridsen E, et al. X-ray diffraction contrast tomography: a novel technique for three-dimensional grain mapping of polycrystals. I. Direct beam case. J Appl Crystallogr. 2008;41(2):302–309. doi: 10.1107/S0021889808001684

[6] Larson BC, Levine LE. Submicrometre-resolution polychromatic three-dimensional X-ray microscopy. J Appl Crystallogr. 2013 Feb;46(1):153–164. doi: 10.1107/S0021889812043737

[7] Simons H, King A, Ludwig W. Dark-field x-ray microscopy for multiscale structural characterization. Nat Commun. 2015;6:6098. doi:10.1038/ncomms7098.

[8] Hayashi Y, Hirose Y, Seno Y. Polycrystal orientation mapping using scanning three-dimensional x-ray diffraction microscopy. J Appl Crystallogr. 2015;48:1094–1101. doi: 10.1107/S1600576715009899

[9] Hektor J, Hall SA, Henningsson NA, et al. Scanning 3DXRD measurement of grain growth, stress, and formation of Cu_6Sn_5 around a tin whisker during heat treatment. Materials. 2019;12(3):446. Available from: https://www.mdpi.com/1996-1944/12/3/446

[10] la Bella M, Besselink R, Wright J, et al. Hierarchical synchrotron diffraction and imaging study of the calcium sulfate hemihydrate–gypsum transformation. J Appl Crystallogr. 2023;56:660–672. doi: 10.1107/S1600576723002881

[11] Li W, Sharma H, Kenesei P, et al. Intragranular evolution of slip system strength and activity in titanium using point-focused high-energy diffraction microscopy. In Review. 2025. doi:10.2139/ssrn.5151306.

[12] Henningsson A, Kutsal M, Wright JP, et al. Microstructure and stress mapping in 3D at industrially relevant degrees of plastic deformation. Sci Rep. 2024;14:20213. doi: 10.1038/s41598-024-71006-0

[13] Jacob JB, Wright J, Cordonnier B, et al. Exploiting Friedel pairs to interpret scanning 3DXRD data from complex geological materials. J Appl Crystallogr. 2024 Dec;57(6):1823–1840. doi: 10.1107/S1600576724009634

[14] Nygren KE, Pagan DC, Miller MP. Sub-grain orientation resolution during continuous loading using only far-field HEDM. IOP Conf Ser Mater Sci Eng. 2019 Aug;580(1):012018. doi: 10.1088/1757-899X/580/1/012018

[15] Nygren KE, Pagan DC, Bernier JV, et al. An algorithm for resolving intragranular orientation fields using coupled far-field and near-field high energy X-ray diffraction microscopy. Mater Charact. 2020;165:110366. Available from: https://www.sciencedirect.com/science/article/pii/S1044580319333182

[16] Frewein MPK, Mason J, Maier B, et al. Texture tomography, a versatile framework to study crystalline texture in 3D. IUCrJ. 2024 Sep;11(5):809–820.doi: 10.1107/S2052252524006547

[17] Carlsen M, Malamud F, Modregger P, et al. Texture tomography with high angular resolution utilizing sparsity. J Appl Crystallogr. 2025 Apr;58(2):484–494. doi: 10.1107/S1600576725001426

[18] Li J, Brochu M, Zhao YF. Chapter five - microstructural features in metallic parts made by am. In: Kadkhodapour J, Schmauder S, Sajadi F, editors. Quality analysis of additively manufactured metals. Amsterdam: Elsevier; 2023. p. 173–200. Available from: https://www.sciencedirect.com/science/article/pii/B9780323886642000099.

[19] Malladi SBA, Chen Z, Durga A, et al. Single track versus bulk samples: understanding the grain refinement in inoculated ferritic stainless steels manufactured by powder bed fusion-laser beam. Materialia. 2023;32:101952. Available from: https://www.sciencedirect.com/science/article/pii/S258915292300279X

[20] Margulies L, Winther G, Poulsen HF. In situ measurement of grain rotation during deformation of polycrystals. Science. 2001;291(5512):2392–2394. doi: 10.1126/science.1057956

[21] Poulsen H, Margulies L, Schmidt S, et al. Lattice rotations of individual bulk grains: Part I: 3D X-ray characterization. Acta Mater. 2003;51(13):3821–3830. Available from: https://www.sciencedirect.com/science/article/pii/S1359645403002064

[22] Winther G, Margulies L, Schmidt S, et al. Lattice rotations of individual bulk grains. Part II: correlation with initial orientation and model comparison. Acta Mater. 2004;52(10):2863–2872. Available from: https://www.sciencedirect.com/science/article/pii/S1359645404001223

[23] Liu H, Zhang Y, Wilkin M, et al. 3D in-situ stop action study of recrystallization in additively manufactured 316L stainless steel: reconstruction optimization

and observations. IOP Conf Ser Mater Sci Eng. 2022 Jul;1249(1):012054. doi: 10.1088/1757-899X/1249/1/012054

[24] Chen Y, Tang Y, Collins D, et al. High-resolution 3d strain and orientation mapping within a grain of a directed energy deposition laser additively manufactured superalloy. Scr Mater. 2023;234:115579. Available from: https://www.sciencedirect.com/science/article/pii/S1359646223003032

[25] Zhang Y, Defer M, Liu W, et al. Challenges in characterizing additively manufactured ALSi10Mg using X-ray Laue micro-beam diffraction. IOP Conf Ser Mater Sci Eng. 2024 Aug;1310(1):012023. doi: 10.1088/1757-899X/1310/1/012023

[26] Zhang Y, Ball J, Henningsson A, et al. Unveiling 3D sub-grain residual stresses in as-built additively manufactured steel using scanning 3DXRD. Mater Res Lett. 2025;13(7):700–708. doi: 10.1080/21663831.2025.2502502

[27] Sumarli S, Polatidis E, Malamud F, et al. A downsized laser powder bed fusion device for operando neutron studies: design and experiments. Addit Manuf. 2025;98:104654. Available from: https://www.sciencedirect.com/science/article/pii/S2214860425000181

[28] Kieffer J, Karkoulis D. PyFAI, a versatile library for azimuthal regrouping. J Phys Conf Ser. 2013;425(20):202012. doi: 10.1088/1742-6596/425/20/202012

[29] Ungár T, Borbély A. The effect of dislocation contrast on x-ray line broadening: a new approach to line profile analysis. Appl Phys Lett. 1996 Nov;69(21):3173–3175. doi: 10.1063/1.117951

[30] Warren BE. X-ray diffraction. New York: Dover Publications; 1990.

[31] Ueji R, Tsuchida N, Terada D, et al. Tensile properties and twinning behavior of high manganese austenitic steel with fine-grained structure. Scr Mater. 2008;59(9):963–966. Available from: https://www.sciencedirect.com/science/article/pii/S1359646208005058

[32] Gutierrez-Urrutia I, Zaefferer S, Raabe D. The effect of grain size and grain orientation on deformation twinning in a Fe–22wt.% Mn–0.6wt.% C TWIP steel. Mater Sci Eng A. 2010;527(15):3552–3560. Available from: https://www.sciencedirect.com/science/article/pii/S0921509310001917

[33] Afroz L, Inverarity SB, Qian M, et al. Analysing the effect of defects on stress concentration and fatigue life of L-PBF ALSi10Mg alloy using finite element modelling. Prog Addit Manuf. 2024;9(2):341–359. doi: 10.1007/s40964-023-00457-0

[34] Mostafaei A, Zhao C, He Y, et al. Defects and anomalies in powder bed fusion metal additive manufacturing. Curr Opin Solid State Mater Sci. 2022;26(2):100974. Available from: https://www.sciencedirect.com/science/article/pii/S1359028621000772

[35] Henningsson NA, Hall SA, Wright JP, et al. Reconstructing intragranular strain fields in polycrystalline materials from scanning 3dxrd data. J Appl Crystallogr. 2020 Apr;53(2):314–325. doi: 10.1107/S1600576720001016

[36] Rahman K, Vorontsov V, Dye D. The effect of grain size on the twin initiation stress in a twip steel. Acta Mater. 2015;89:247–257. Available from: https://www.sciencedirect.com/science/article/pii/S1359645415001081